

Article

Implementation of Magnetic Nanostructured Adsorbents for Heavy Metals Separation from Textile Wastewater

Marco Barozzi ¹, Sabrina Copelli ¹, Eleonora Russo ², Paolo Sgarbossa ² , Maria Cristina Lavagnolo ³ , Annalisa Sandon ³ , Cristiana Morosini ¹  and Elisabetta Sieni ^{4,*} 

- ¹ Department of Science and High Technology, University of Insubria, via Valleggio 9, 22100 Como, Italy
² Department of Industrial Engineering, University of Padova, via F. Marzolo 9, 35131 Padova, Italy
³ Department of Civil, Environmental and Architectural Engineering, University of Padova, via F. Marzolo 9, 35131 Padova, Italy
⁴ Department of Theoretical and Applied Sciences, University of Insubria, via Jean Henry Dunant 3, 21100 Varese, Italy
* Correspondence: elisabetta.sieni@uninsubria.it

Abstract: In the framework of sustainability, water shortages and water pollution are two important aspects to be considered. Proposing efficient and low-impact technologies is of paramount importance to promote circular economies associated with the use of water in the industrial context, especially in the textile industry. In this work, the application of a set of magnetic nanostructured adsorbents (MNAs) to cleanse metal ions from textile wastewaters was studied and analyzed. MNAs were generated with a low-cost process, involving iron (II/III) salts (e.g., chlorides), sodium or ammonium hydroxide solutions, and graphene oxide, obtained from graphite by a modified Hummers' method at room temperature. The shape and the size were studied with transmission electron microscopy. Adsorbents were tested with different metal ions (e.g., copper, chromium (III), and nickel). Metal ion concentrations were analyzed by means of inductively coupled plasma optical emission spectroscopy (ICP-OES), and adsorption isotherms were characterized. From the results, the MNAs exhibited the capability of removing metal ions up to a yield of 99% for Cr³⁺, 94.7% for Cu²⁺, and 91.4% for Ni²⁺, along with adsorption loads up to 4.56 mg/g of MNAs.

Keywords: wastewater; adsorption; nanoadsorbents; graphene oxide; magnetic nanoparticles



check for updates

Citation: Barozzi, M.; Copelli, S.; Russo, E.; Sgarbossa, P.; Lavagnolo, M.C.; Sandon, A.; Morosini, C.; Sieni, E. Implementation of Magnetic Nanostructured Adsorbents for Heavy Metals Separation from Textile Wastewater. *Sustainability* **2022**, *14*, 11785. <https://doi.org/10.3390/su141811785>

Academic Editors: Bo Chen, Guohua Dao and Zhiliang Cheng

Received: 27 July 2022

Accepted: 14 September 2022

Published: 19 September 2022

Publisher's Note: MDPI stays neutral with regard to jurisdictional claims in published maps and institutional affiliations.



Copyright: © 2022 by the authors. Licensee MDPI, Basel, Switzerland. This article is an open access article distributed under the terms and conditions of the Creative Commons Attribution (CC BY) license (<https://creativecommons.org/licenses/by/4.0/>).

1. Introduction

Water is one of the most important and strategic resources for human life, industry, and the environment. It is estimated that, globally, only 10% of the available water is for domestic use. According to the World Health Organization and UNICEF, about 768 million people do not have access to clean water [1]. Climate change is also contributing to the reduction of water for mankind. According to the report “*Climate Change: Impacts, Adaptation and Vulnerability*” [2], 80% of the world suffers from water scarcity [3], and this number is unfortunately destined to increase. The European Environmental Agency (EEA) constantly promotes the development and application of sustainable technologies, through the State of Environment reporting (SOER), a yearly report which describes, for each Eionet country (26 in total), topics related to environmental issues and solutions.

In this framework, wastewater takes a huge part in water wastes, being involved in the food, agricultural [4], fine chemical, oil, textile [5], and pharmaceutical industries. Currently, wastewater management in Europe is performed through the definition of threshold limit values of pollutant concentrations in water for human use, defined within dedicated standards (European Council Directives 91/271/EEC and 98/15/EC). Pollutant distribution is usually non-homogeneous, and highly dependent on specific anthropogenic activities across the territory. Focusing on textile industry wastewater, with the widespread use of dyes, a huge presence of both organic substances and nickel (II), copper (II), and

chromium (III) ions [6] can be traced. The EEA constantly monitors the factors involved in the water pollution assessment, developing reports based upon communications from each member of the European Union. According to the EEA [7], which reports the presence and the distribution of water pollutants in different activities, heavy metals constitute an important component of wastewater, with more than 1400 tons estimated in 2018 [7].

In addition, according to the EEA [7], in 2016 more than 34,000 facilities transferred data to the European Pollutant Release and Transfer Register; however, only a relatively small fraction of these (3600) contained references to water emissions. This is due to the fact that all facilities having pollutant releases below the threshold limit values do not have an obligation to communicate the emission data. This fact highlights the importance of promoting new and efficient wastewater treatment systems and technologies.

Currently, the most-used methods for wastewater treatment include ultrafiltration, flocculation, coagulation [8], adsorption methods and, for organic pollutants only, biological processes [9]. Focusing on the removal of heavy metal compounds from wastewater, chemical methods are available, but they are generally expensive and they show a poor removal efficiency at full-plant scale [10]. On the contrary, adsorption is considered an optimal chemical–physical method of removal, as it is easy to operate, cost-effective, and efficient for both organic and inorganic substances in aqueous media [10]. In recent years, environmental remediation research studies have been focused on the design and development of nanosized materials for adsorption [6]. According to the International Organization for Standardization, a nanomaterial is defined as a ‘material with any external dimensions in the nanoscale or having internal structure or surface structure in the nanoscale’. The term ‘nanoscale’ is defined as size range from approximately 1 nm to 100 nm [11]. Such dimensions typically offer to nanomaterials peculiar properties, namely a high surface area/volume ratio. In fact, if compared to massive material, the number of surface atoms and their properties make them the best candidates as adsorption systems. On the one hand, their small size allows a low resistance to mixing but, on the other, it makes it difficult to remove them from aqueous solutions with traditional separation technologies [12]. For such reasons, adding properties such as magnetism to the nanoadsorbent allows for the implementation of magnetic separation, a technology largely used in the mineral industry and foundries to separate magnetic ores from non-magnetic materials [13]. The same method has been proposed to extract pollutants from liquids using magnetic nanostructured adsorbents (MNAs) [14]. To achieve such a target, a static magnetic field is used to separate and extract the magnetic part from the fluid [15]. This technique is particularly efficient, as it avoids the use of filters or membranes that can lead to related fouling problems [16]. In recent years, much research has been carried out into the use of MNAs for water pollutants. Among magnetic materials, iron oxide is naturally abundant in nature in the forms of magnetite, Fe_3O_4 and maghemite, $\gamma\text{-Fe}_2\text{O}_3$. As nanoparticles, they have good removal properties toward heavy metals through different processes such as adsorption, reduction, and co-precipitation (Figure 1). Most of the studies in this area use iron oxide as the base to grant magnetic properties to the nanoparticles. Depending on the substrate, magnetite and maghemite nanoparticles are involved in both physical and chemical adsorption (including hybrid mechanisms), with maghemite usually involving physical adsorption when used on heavy metals [17–19].

This is also demonstrated by the low desorption of metals at high pH, that occurs when applying magnetite, Fe_3O_4 , nanoparticles, typical of chemical adsorption [20]. Instead, adsorption by $\gamma\text{-Fe}_2\text{O}_3$ nanoparticles does not involve chemical reaction as demonstrated by the unchanged crystallite structure after metal removal [21]. Mahdavian et al. [22] have investigated the ability of magnetite nanoparticles functionalized with APTES (3-aminopropyl-triethoxysilane) and acryloyl chloride to adsorb heavy metal cations such as Cd^{2+} , Pb^{2+} , Ni^{2+} , and Cu^{2+} . The adsorption capacity was maximum for lead ions and minimum for cadmium ions. Ozmen et al. [23] have studied the capacity of magnetite nanoparticles functionalized with APTES and glutaraldehyde to remove Cu^{2+} from water.

They reached adsorption equilibrium in 15 min and found that the removal is pH dependent, with maximum removal at a pH between 4 and 5.

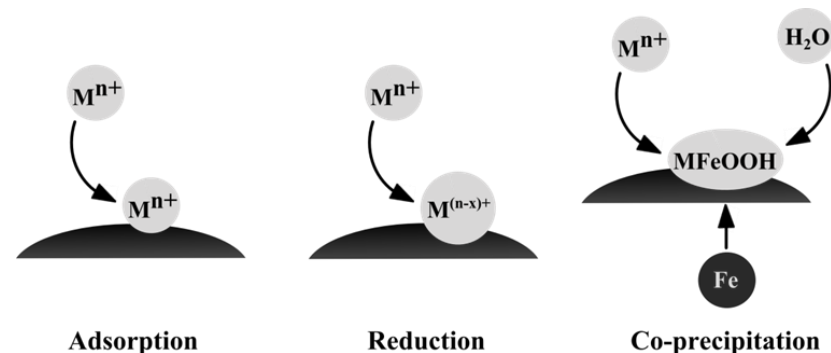


Figure 1. Metal ion removal with MNAs.

However, even if magnetism increases separation yield of MNAs, their complete separation from the aqueous matrix is still difficult. This issue can be partially solved by supporting the nanoparticles onto other materials with high surface areas but with at least one non-nanometric dimension (e.g., carbon nanotubes or nanosheets). Among 2D nanomaterials, graphene oxide (GO) is an ideal candidate thanks to: (i) its large surface area and (ii) the presence of both hydrophobic sp^2 -hybridized domains [24] and hydrophilic ones (bearing hydroxy, ether, and carboxylic groups [25]) allowing for the adsorption of both organic and inorganic pollutants such heavy metals [26]. The many advantages of GO include: (i) hydrophilicity/hydrophobicity; (ii) easy and cost-effective production as GO is easily produced from graphite, that is abundant in nature; (iii) adsorption capacities similar to those of zeolites [27]; (iv) availability of functional groups that can be either chemically modified or used as binding sites for metal cations; and (v) high surface area per mass unit.

Graphene-oxide-based composite materials have been extensively studied as adsorbents due to their strong affinity and high efficiency toward metal ions [28]. The formation of composites between GO and magnetic nanoparticles represents a winning strategy for the recovery of both nanomaterials after the decontamination treatment [29], as proved by Diagboya et al. [30].

In fact, magnetic nanocomposites allow for the implementation of a green treatment system, as the separation of the adsorption medium can be easily performed by the application of a magnetic field or by using a simple magnet [31].

This work aims to propose a new set of MNAs, with the potential capability of removing very different metal ions one-pot (that is, at the same time, in the same vessel).

The nanoadsorbent used in this work is based on GO decorated with magnetite nanoparticles and it was synthesized by taking advantage of the high surface area of GO and the cost-effective one-step coprecipitation method. This method makes use of cheap iron (II/III) salts (e.g., chlorides) and a base (sodium or ammonium hydroxide solution) to decorate a dispersion of GO in water at room temperature. The main advantage in the proposed system as compared to other state-of-the-art carbon-based adsorbents [32] stems from the use of a very simple synthetic procedure and making use of GO and NPs without further functionalization. In fact, the latter can impart specific affinity for certain heavy metals but add complexity to the synthesis and limit its scalability.

Some preliminary results on the removal of Cr^{3+} ions only by similar MNAs have been reported earlier by Barozzi et al. [33], but no adsorption isotherms have been proposed.

The nanoadsorbent used in this work was tested on three different pollutants: Cr^{3+} , Ni^{2+} , and Cu^{2+} . Such pollutants are typical of wastewater from textile industry [34]. MNAs were tested with different starting concentrations (within the range 400–6000 $\mu\text{g}/\text{mL}$), from which adsorption isotherms were proposed. From the isotherms, specific parameters were fitted using a Langmuir model.

2. Materials and Methods

All the methods and techniques used are explained in detail in the following section.

2.1. MNA Production and Characterization

The magnetic nano-adsorbent based on Fe_3O_4 -NPs-decorated GO was prepared by a simple coprecipitation method [35] in the presence of graphene oxide. The production scheme is summarized in Figure 2. GO was obtained from graphite by a modified Hummers' method [36] at room temperature. In a typical procedure (Figure 2), 340 mg of $\text{FeCl}_2 \cdot 4\text{H}_2\text{O}$ and 965 mg of $\text{FeCl}_3 \cdot 6\text{H}_2\text{O}$ (resulting in 350 mg of Fe_3O_4) were mixed with 5 mL of GO suspension (10 g/L, 50 mg) in 50 mL of distilled water. The mixture was stirred for 30 min at room temperature to completely dissolve the iron salts and then treated with 7 mL of NH_4OH solution (25% in water) under vigorous stirring, to rapidly increase the pH to 11. After 1 h of continuous stirring, the nanocomposite was magnetically separated from the solution, washed with distilled water until neutrality, then with ethanol to remove the water, and dried under vacuum.

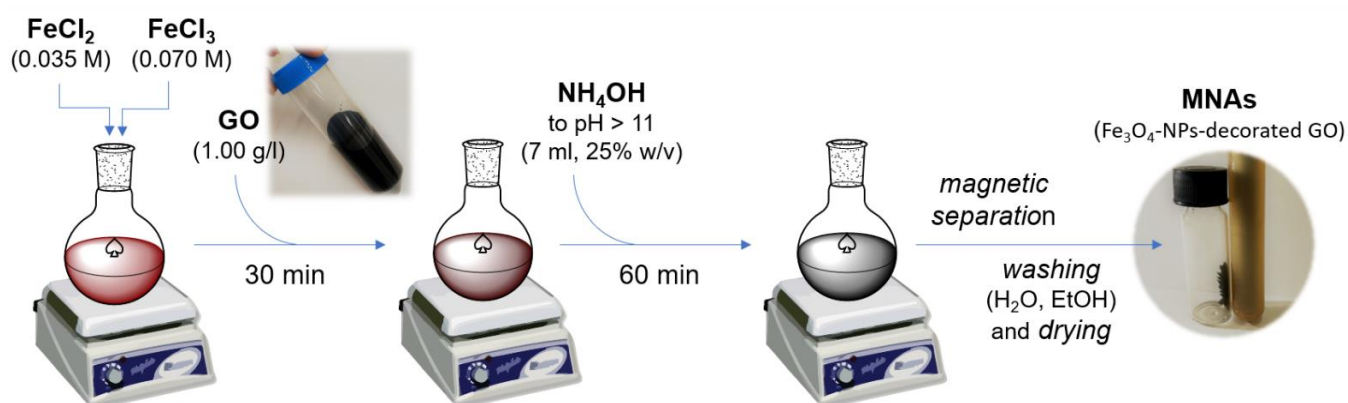


Figure 2. Synthesis of the MNAs.

The MNAs were characterized by transmission electron microscope (TEM) analysis using a TEM FEI Tecnai G12 (FEI—Thermo Fischer Scientific, Hillsboro, OR, USA) instrument, operating at 100 KV at the Electron Microscopy Laboratories (LME) of the Department of Biology, University of Padova. The sample was prepared by depositing a water-suspension drop of the nanomaterial on 400 mesh carbon-coated copper grids.

2.2. MNA Testing

The MNAs developed were tested with three different heavy metal ions:

- Cu^{2+} (copper (II) sulphate, $\text{CuSO}_4 \cdot 5\text{H}_2\text{O}$, 99% Sigma Aldrich, St. Louis, MO, USA)
- Ni^{2+} (nickel (II) chloride, $\text{NiCl}_2 \cdot 6\text{H}_2\text{O}$, 99% Sigma Aldrich)
- Cr^{3+} (chromium (III) chloride, $\text{CrCl}_3 \cdot 6\text{H}_2\text{O}$, 99% Sigma Aldrich)

Such pollutants are typical of the textile industry, and they are subject of many recent literature works [37–40].

MNAs were tested with different sets of concentrations. In particular, for chromium (III), 500, 600, 1000, 2000, and 5000 $\mu\text{g}/\text{L}$ concentrations were tested; for copper (II), 300, 500, 700, 1000, 2000, and 6000 $\mu\text{g}/\text{L}$ concentrations were tested; and, finally, for nickel (II), 1000, 2000, 4000, and 5000 $\mu\text{g}/\text{L}$ concentrations were used. These concentrations are comparable with the values found in wastewater coming from textile industries; this is also the reason for the non-standardized range of the tested concentrations.

Tests were performed in a stirred lab glass flask (100 mL nominal volume for chromium and 50 mL for nickel and copper) at 298 K. Keeping stirring speed as low as possible is an important aspect, as MNAs may be compromised by an excessive mechanical stress. For

chromium tests, 50 mL of solution was used. For nickel and copper, 20 mL of solution was abated. MNAs content was 1 g/L for each test.

After loading MNAs in the solution, the vessel was kept at 298 K and stirred for 30 min. MNA filtration was finally carried out by using a classic neodymium magnet. The treated liquid was also filtered to eliminate eventual traces of adsorbents. Concentration measurements were carried out by inductively coupled plasma optical emission spectroscopy (ICP-OES) on a Perkin Elmer Optima 4200 DV (Perkin Elmer Italia S.p.A., Milano, Italy).

Every test was performed according to the following protocol: (a) solution preparation at target concentration, (b) preparation of the blank sample for starting concentration measurement, (c) loading of water in the flask, (d) loading of the MNAs, (e) stirring at 100 rpm for 30 min (to ensure the reaching of the adsorption equilibrium), (f) MNA separation (magnet + filtration), and (g) preparation of sample for final concentration measurement.

Finally, the removal efficiency was tested in six mixtures obtained mixing the three ions at different concentrations. For each mixture 20 mL of solution was treated as for the tests of single ion solutions, using MNAs at 1 mg/mL.

Adsorption Isotherms

Basing on the difference between initial and final ions concentrations, the corresponding adsorption isotherms were developed. All the adsorption parameters were fitted from the experimental data according to a Langmuir model, which was expected to give the best performances in terms of physical description of the adsorption process even if such a model was originally developed for the description of gas adsorption on solid phases as activated carbons [40]. According to the Langmuir theory, the adsorption process onto a solid surface is based on a kinetic principle in which a continuous bombardment process of molecules onto the surface with corresponding molecules desorption (or evaporation) from the surface, with zero accumulation rate at the surface, occurs [41]. Practically, the rates of adsorption and desorption should be equal (equilibrium conditions).

Such an adsorption model is very versatile and can be simply extended to characterize different adsorption processes, such as the adsorption of metal ions dissolved in aqueous solutions on MNAs.

The Langmuir isotherm model can be described by Equation (1):

$$\eta_{eq} = \frac{Q_{eq} \cdot b_{eq} \cdot C_e}{1 + b_{eq} \cdot C_e} \quad (1)$$

where Q_{eq} and b_{eq} are constants, C_e represents the equilibrium concentration of the compound to be removed from the fluid phase, and η_{eq} is the equilibrium load of the same compound onto the adsorbent. Obtaining effective equilibrium conditions (both for fluid and solid phases) is experimentally very difficult as it requires a constant compound concentration in the fluid phase until the maximum load onto the solid phase at that compound concentration is reached.

Because of this feature, modified adsorption isotherms have been proposed throughout the scientific literature.

In particular, referring to the adsorption of different metal ions (that is, copper, chromium, and nickel) on the MNAs dispersed into an aqueous solution, Equation (1) can be modified as follows (Equation (2)):

$$\eta_{end} = \frac{Q_{max} \cdot b \cdot C_0}{1 + b \cdot C_0} = \frac{(C_{end} - C_0) \cdot V_{sol}}{m_{MNAs}} \quad (2)$$

where Q_{max} and b are constants, C_0 represents the initial concentration of the metal ion(s) ($\mu\text{mol/L}$) into the analyzed solution (fluid phase), C_{end} is the concentration of metal ion(s) in fluid phase at the end of the treatment, V_{sol} is the volume of the aqueous solution (L), m_{MNAs} is the mass of MNAs used for a single treatment (mg), and η_{end} is the final load of

metal ion(s) which is adsorbed onto the MNAs ($\mu\text{mol}/\text{mg}$). The removal (or adsorption) efficiency, χ , is evaluated as it follows (Equation (3)):

$$\chi = \frac{C_0 - C_{end}}{C_0} \quad (3)$$

Isotherm-specific parameters were fitted according to a non-dominated sorting genetic algorithm, NSGA-II [42]. The design variables to be found (Q_{max} and b) are the coefficients of the Langmuir function in Equation (2).

These values were designed to minimize two objective functions: f_1 (Equation (4)), the sum of the square of the point-to-point difference of the N measured values with respect to the ones evaluated by Equation (2) at different concentration of the initial solution $[C_0]$ $I = 1, \dots, N$, and, f_2 (Equation (5)), the minimization of the maximum of the point-to-point discrepancy between the measured values and the ones evaluated by the model in Equation (2). Then, the optimization problem is based on the following objective functions, to be minimized:

$$f_1 = \sum_{i=1}^N \left(X_{m,i}([C_{0,i}]) - X_{f,i}([C_{0,i}]) \right)^2 \quad (4)$$

$$f_2 = \max_{i=1, \dots, N} \left(\left| X_{m,i}([C_{0,i}]) - X_{f,i}([C_{0,i}]) \right| \right) \quad (5)$$

where X_m is the experimental value of η_{end} as derived from the right side of Equation (2) and X_f is the value of η_{end} as estimated by the Langmuir model (that is, the left side of Equation (2)). The optimization problem is solved by using a genetic algorithm in the class of non-dominated sorting genetic algorithm, NSGA-II [43]. In particular, the modified version in which the periodic migration of sub-population is considered was applied.

This algorithm considers an initial population of $N_i = 40$ individuals, the set of $N_d = 2$ design variables, and a $1 \times$ array of N_d values, that combine between themselves in order to obtain a child population added to the original population (up to $2 N_i$ individuals). Using a selection operator, a set of 40 individuals, the best ones, in terms of minimization of the two objective functions f_1 and f_2 , are selected to survive and the algorithm iterate to generate a new population. The algorithm stops after 200 iterations. The solutions on the Pareto front represent the improved solutions in terms of objective functions.

3. Results and Discussion

In the following, results concerning the production and the application of MNAs are reported.

3.1. MNA Characterization

Figure 3 reports the TEM images of the MNAs at different magnifications. The GO nanosheets had irregular shapes and sizes ranging from 200 to 500 nm. The MNAs were composed of a few sheets of GO with bounded magnetic nanoparticles which were not evenly distributed in the GO surface but tended to form aggregates closer to the sheet's borders, leaving wide sections of the surface areas of GO free for adsorption. The magnetite NPs generally showed a rounded shape, and a granulometric size distribution centered around 7.2 nm (standard deviation = 2.4 nm; about 300 NPs were measured).

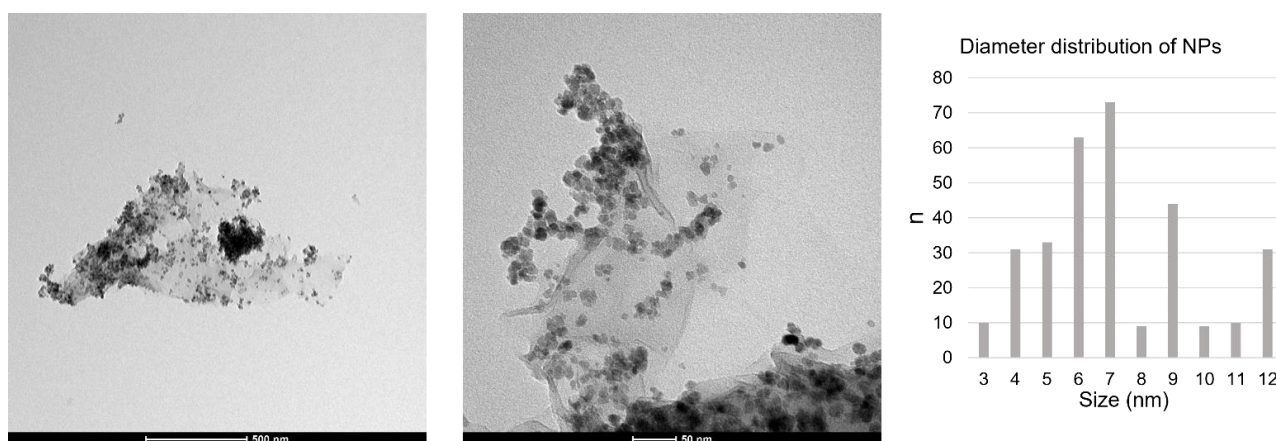


Figure 3. TEM images of the MNA nanosheets and size distribution of the magnetite nanoparticles.

3.2. MNA Isotherm Evaluation

For the selected ions, the isotherms were experimentally evaluated. All tests were performed, in triplicate, at 298 K. Table 1 reports in detail the results for chromium (III). With ion concentrations below 1100 $\mu\text{g/L}$, the adsorption efficiency was always above 0.97, showing that the equilibrium state was reached at higher removal-efficiency values. Above 1100 $\mu\text{g/L}$, χ decreased progressively till reaching values of less than 0.45 for 5000 $\mu\text{g/L}$ (where a maximum load of 2.23 mg/g was reached). Compared with other literature works using different adsorbents [36,37], the adsorption capacity was relatively low, but in these works concentrations up to 50 ppm were tested; which very different to the values tested in the present work (up to 5 ppm). In addition, all tests were performed at neutral pH, so it was not required to adjust it to achieve an optimal adsorption.

Table 1. Concentrations, load, and removal efficiency for chromium (III) tests.

Cr^{3+}	#1	#2	#3	#4	#5
C_0 , $\mu\text{g/L}$	440 ± 1	580 ± 1	1060 ± 10	1810 ± 10	4990 ± 10
C_{end} , $\mu\text{g/L}$	10 ± 1	10 ± 1	17 ± 1	370 ± 1	2760 ± 10
η_{end} , mg/g	0.43	0.57	1.04	1.44	2.23
X , -	0.977	0.983	0.984	0.796	0.447

For copper, the main results are reported in Table 2. Results were similar to chromium, but efficiency appeared to be lower at low starting concentrations. This may have been due to a minor residue of MNAs not entirely removed from the treated water. At 6.43 mg/L of Cu^{2+} concentration, the adsorption capacity was 4.56 mg/g, with a removal efficiency equal to 0.710. The adsorption capacity was comparable to other works [39], considering the neutral pH.

Table 2. Concentrations, load, and removal efficiency for copper (II) tests.

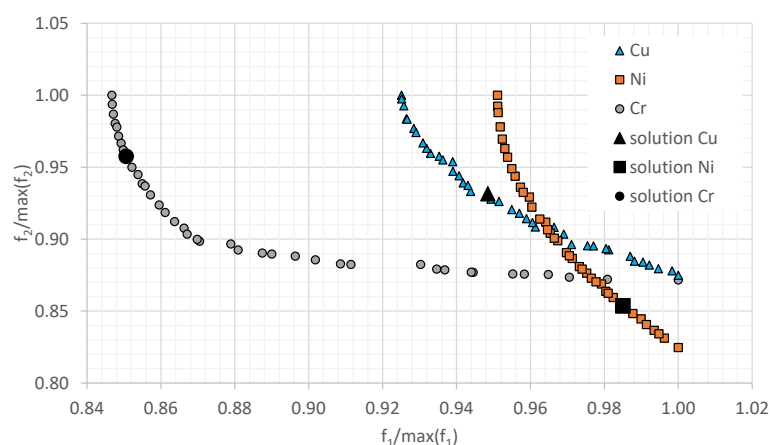
Cu^{2+}	#1	#2	#3	#4	#5	#6
C_0 , $\mu\text{g/L}$	296 ± 1	501 ± 1	690 ± 1	1020 ± 10	2000 ± 10	6430 ± 10
C_{end} , $\mu\text{g/L}$	26 ± 1	45 ± 1	49 ± 1	54 ± 1	185 ± 1	1865 ± 10
η_{end} , mg/g	0.27	0.46	0.64	0.97	1.81	4.56
X	0.912	0.910	0.930	0.947	0.907	0.710

Finally, results for nickel are reported in Table 3. Adsorption efficiency steadily increased with initial concentrations, with 0.914 at 935 $\mu\text{g/L}$ and 0.566 at 5120 $\mu\text{g/L}$ starting concentrations. The maximum achieved load of nickel (II) ions was found to be 2.90 mg/g, which was higher than that for chromium under similar starting concentrations. Even in this case, results were similar to the ones reported in other works [39].

Table 3. Concentrations, load, and removal efficiency for nickel (II) tests.

Ni ²⁺	#1	#2	#3	#4
C ₀ , µg/L	935 ± 1	1900 ± 10	3980 ± 10	5120 ± 10
C _{end} , µg/L	80.4	298	1700	2220
η _{end} , mg/g	0.85	1.60	2.28	2.90
X	0.914	0.843	0.573	0.566

Given the experimental results of absorption efficiency, the parameters of Equation (2) were evaluated solving the optimization problem. Figure 4 represents the f_1 - f_2 diagram, the Pareto fronts found using NSGA-II, for the three analyzed elements, Cu, Ni, and Cr, normalized to the maximum of the function obtained by minimizing the objective functions in Equations (4) and (5). Each point in the diagram corresponds a set of values for the design variables. In each front the black points represent the trade-off set of design variables. The values of two of the design variables are reported in Table 4 and used to fit the experimental data by means of the Langmuir function. Table 4 reports the Langmuir parameters. The Langmuir function showed a very good agreement with experimental data, showing a minimizing function f_1 always lower than $2 \cdot 10^{-5}$. The correlation coefficient was also always equal or greater than 0.99. This aspect evidences a single-layer adsorption, which is well-described by the Langmuir model. The maximum monolayer adsorption capacity ranged between 3.42 and 31.3 mg/g (MNA). The maximum value of adsorption load was found for copper (II), with a significant greater compatibility with the nanoparticles studied.

**Figure 4.** Pareto fronts for the three ions normalized to the maximum of the objective function. Black points represent the objective values corresponding to the chosen solution.**Table 4.** Langmuir and fitting parameters from NSGA-II optimization algorithm for the investigated ions.

	Cr ³⁺	Cu ²⁺	Ni ²⁺
Q _{max} [mg/g(MNA)]	3.42	31.3	5.45
b [L/mg]	0.38	2.75 · 10 ⁻²	0.20
f ₁	3.92 · 10 ⁻⁶	1.74 · 10 ⁻⁵	1.39 · 10 ⁻⁵
f ₂	1.21 · 10 ⁻³	2.86 · 10 ⁻³	2.44 · 10 ⁻³
R ²	0.9978	0.9987	0.9900

Figure 5 shows the results of the fitting of the Langmuir isotherm of the experimental data. The results, which were in accordance to the Langmuir hypothesis, highlight the prevalence of monolayer adsorption as the controlling mechanism for the adsorbent tested. According to Figure 5, it is reasonable to assume that Cu adsorption capacity may have increased still further at higher concentration values.

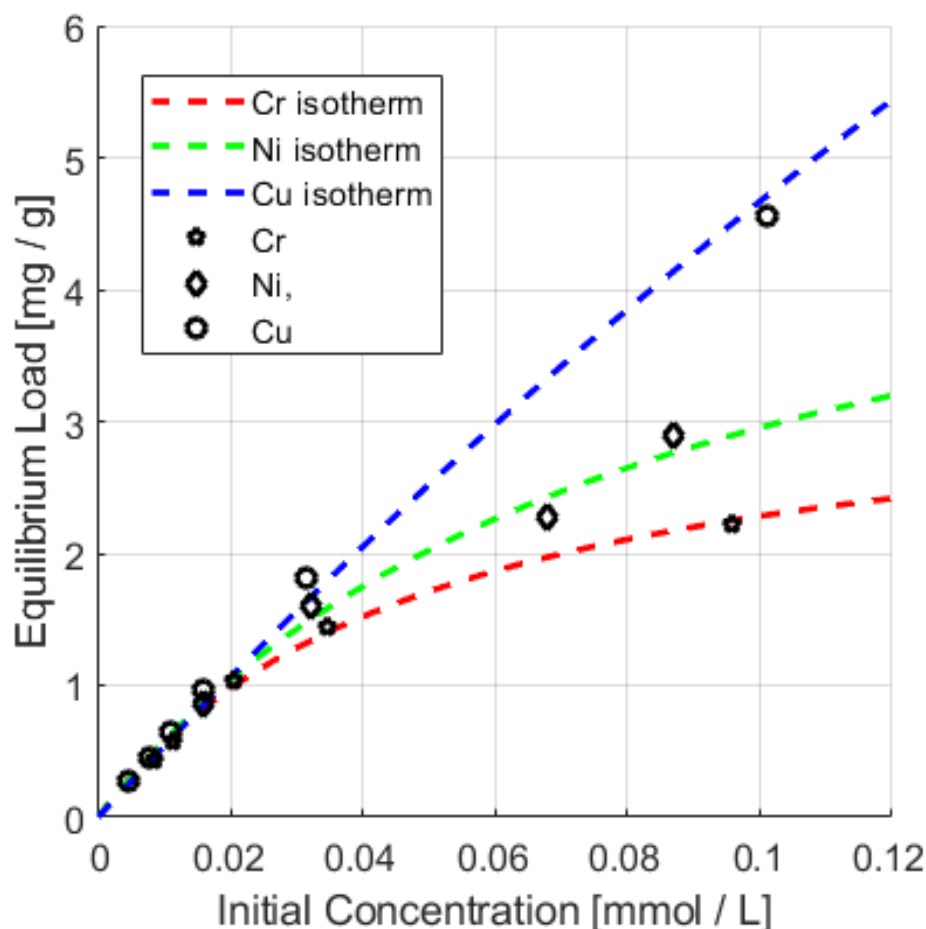


Figure 5. Comparison among different ions with same MNA concentration (1 mg/mL) and temperature (298 K).

To carry out a preliminary test of the reliability of the previously proposed isotherms, six different mixtures of the three tested ions were prepared. The initial composition of the mixtures together with the results obtained after the treatment with 1 mg/mL of MNAs are reported in Table 5.

Table 5. Data for chromium (III), nickel (II), and copper (II) removal and equilibrium loads.

#	$C_{0,Cr}$ [$\mu\text{g}_{Cr}/\text{L}$]	$C_{0,Cu}$ [$\mu\text{g}_{Cu}/\text{L}$]	$C_{0,Ni}$ [$\mu\text{g}_{Ni}/\text{L}$]	χ_{Cr} -	χ_{Cu} -	χ_{Ni} -	$\eta_{end,Cr}$ [$\mu\text{g}_{Cr}/\text{mg}$]	$\eta_{end,Cu}$ [$\mu\text{g}_{Cu}/\text{mg}$]	$\eta_{end,Ni}$ [$\mu\text{g}_{Ni}/\text{mg}$]
(a)	430 ± 1	293 ± 1	937 ± 1	0.977	0.927	0.859	0.42	0.63	0.81
(b)	1830 ± 10	316 ± 1	1030 ± 10	0.888	0.809	0.645	1.625	0.140	0.665
(c)	1860 ± 10	500 ± 1	1850 ± 10	0.812	0.827	0.539	1.51	0.222	0.997
(d)	4540 ± 10	1050 ± 10	5090 ± 10	0.454	0.680	0.167	2.06	0.157	0.85
(e)	4690 ± 10	317 ± 1	1060 ± 10	0.480	0.769	0.334	2.25	0.052	0.354
(f)	1830 ± 10	987 ± 1	5100 ± 10	0.849	0.854	0.284	1.55	0.461	1.45

Figure 6 reports the comparison among experimental data (see Table 5) and predicted values of the ion(s) load on the selected magnetic nanoparticles (NP).

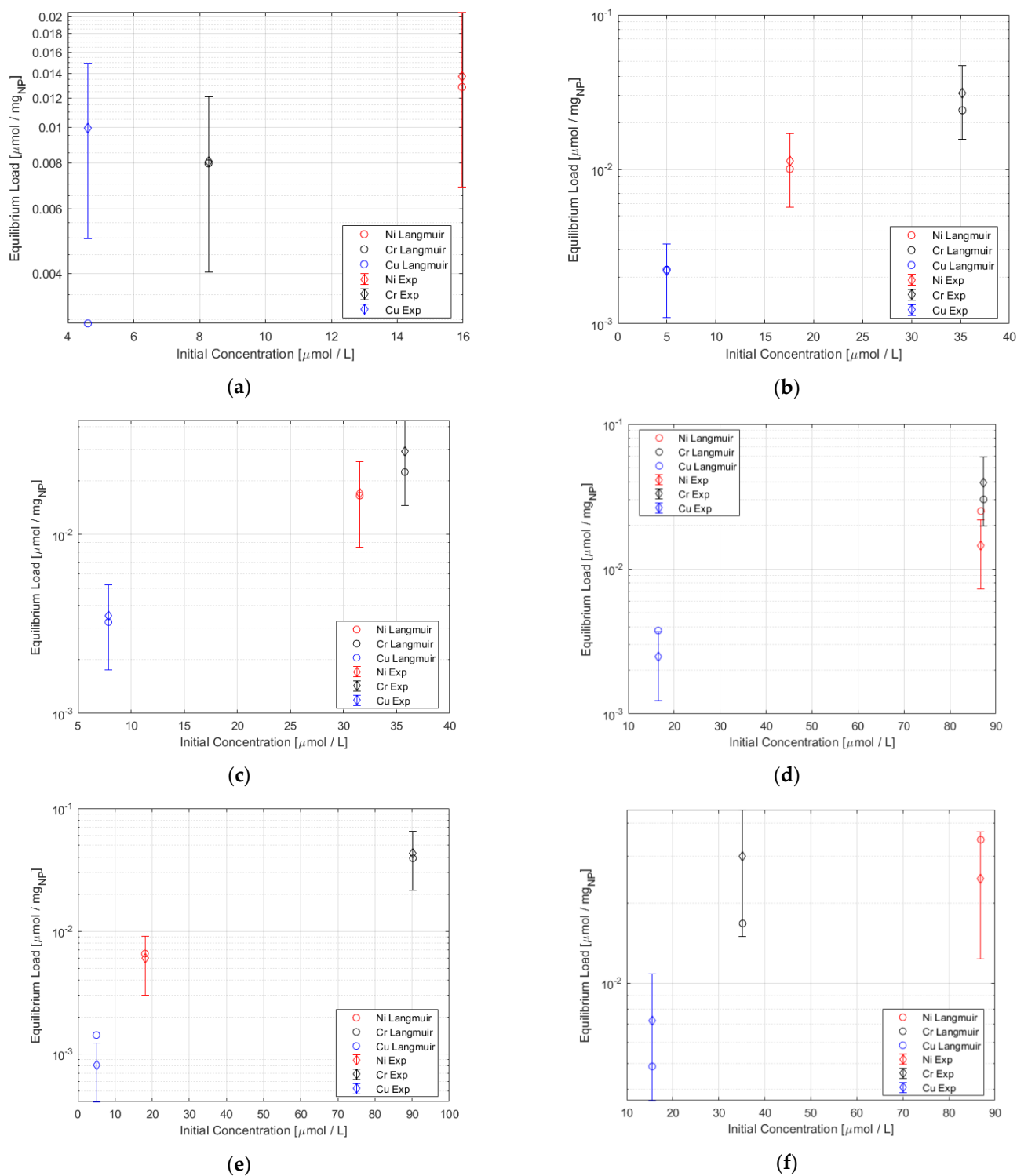


Figure 6. Comparison among experimental and predicted data for the six ion mixtures detailed in Table 5. Starting concentrations: (a) 430 $\mu\text{g}/\text{L}$ (Cr), 293 $\mu\text{g}/\text{L}$ (Cu), 937 $\mu\text{g}/\text{L}$ (Ni), (b) 1830 $\mu\text{g}/\text{L}$ (Cr), 316 $\mu\text{g}/\text{L}$ (Cu), 1030 $\mu\text{g}/\text{L}$ (Ni), (c) 1860 $\mu\text{g}/\text{L}$ (Cr), 500 $\mu\text{g}/\text{L}$ (Cu), 1850 $\mu\text{g}/\text{L}$ (Ni), (d) 4540 $\mu\text{g}/\text{L}$ (Cr), 1050 $\mu\text{g}/\text{L}$ (Cu), 5090 $\mu\text{g}/\text{L}$ (Ni), (e) 4690 $\mu\text{g}/\text{L}$ (Cr), 317 $\mu\text{g}/\text{L}$ (Cu), 1060 $\mu\text{g}/\text{L}$ (Ni), (f) 1830 $\mu\text{g}/\text{L}$ (Cr), 987 $\mu\text{g}/\text{L}$ (Cu), 5100 $\mu\text{g}/\text{L}$ (Ni).

As can be seen from Figure 6, all the equilibrium loads predicted using a competitive Langmuir isotherm for the three ions gave results within the range of the experimental uncertainty (which was 0.5 times the measured value). Minor deviations were found

for copper only, precisely for mixtures (a) and (e), where the Langmuir model predicted, respectively, lower and higher loads with respect to the experimental evidence. Such a behavior could be due to the high affinity of copper ions for the proposed MNAs.

4. Conclusions

In this study, magnetic nanostructured adsorbents were developed and tested for the removal of different metal ions (Cr^{3+} , Ni^{2+} , and Cu^{2+}) at 298 K. From these data, single adsorption isotherms were determined and, successively, tested with six different mixtures of the three studied metal ions. The maximum overall adsorption efficiencies obtained when testing single-ion solutions were over 98% for chromium (III), 94% for copper (II), and 91% for nickel (II). Regarding the mixtures of the three different ions, the maximum removal efficiencies slightly decreased for nickel (II) (maximum 86%) but seemed to be not affected for chromium (III) and copper (II).

The capacity for removing one-pot a mix of pollutant is an extremely valuable feature for wastewater treatment, as real samples are indeed made of a mix of pollutants rather than a single component. The proposed MNAs showed a good removal efficiency even using very different mixtures of Cr^{3+} , Ni^{2+} , and Cu^{2+} and the predictions using a competitive Langmuir model were confirmed by the experimental tests.

Both synergistic and antagonistic effects should be further investigated in future studies, even considering the dynamic adsorption behavior of different metal ions.

Author Contributions: Conceptualization, C.M., E.S. and S.C.; methodology, S.C. and P.S.; validation, M.B., A.S. and M.C.L.; formal analysis, M.B. and A.S.; investigation, S.C., P.S. and E.R.; resources, M.C.L., E.S. and A.S.; data curation, M.C.L.; writing—original draft preparation, M.B., S.C. and P.S.; writing—review and editing, E.S., M.B. and S.C.; visualization, S.C. and P.S.; supervision, P.S. and E.S.; project administration, M.B., S.C. and A.S. All authors have read and agreed to the published version of the manuscript.

Funding: This research received no external funding.

Institutional Review Board Statement: Not applicable.

Informed Consent Statement: Not applicable.

Acknowledgments: The authors wish to thank Leonardo Giusti for the technical support during the adsorption tests. The authors wish to acknowledge Andrea Re and Elisabetta Zanardini for the support given during the early stage of research conceptualization.

Conflicts of Interest: The authors declare no conflict of interest.

References

1. WHO/UNICEF Progress on Sanitation and Drinking-Water—Update 2013. Available online: <https://apps.who.int/iris/handle/10665/81245> (accessed on 28 August 2022).
2. IPCC AR5 Climate Change 2014: Impacts, Adaptation, and Vulnerability. Available online: <https://www.ipcc.ch/report/ar5/wg2/> (accessed on 28 August 2022).
3. Jaspal, D.; Malviya, A. Composites for Wastewater Purification: A Review. *Chemosphere* **2020**, *246*, 125788. [CrossRef] [PubMed]
4. Wang, Y.; Serventi, L. Sustainability of Dairy and Soy Processing: A Review on Wastewater Recycling. *J. Clean. Prod.* **2019**, *237*, 117821. [CrossRef]
5. Chandanshive, V.; Kadam, S.; Rane, N.; Jeon, B.-H.; Jadhav, J.; Govindwar, S. In Situ Textile Wastewater Treatment in High Rate Transpiration System Furrows Planted with Aquatic Macrophytes and Floating Phytobeds. *Chemosphere* **2020**, *252*, 126513. [CrossRef] [PubMed]
6. Ali, I.; Basheer, A.A.; Mbianda, X.Y.; Burakov, A.; Galunin, E.; Burakova, I.; Mkrtychyan, E.; Tkachev, A.; Grachev, V. Graphene Based Adsorbents for Remediation of Noxious Pollutants from Wastewater. *Environ. Int.* **2019**, *127*, 160–180. [CrossRef]
7. European Environment Agency EEA Report No 23/2018 Industrial Waste Water Treatment Pressures on Environment. Available online: <https://www.eea.europa.eu/publications/industrial-waste-water-treatment-pressures> (accessed on 28 August 2022).
8. Lee, K.E.; Morad, N.; Teng, T.T.; Poh, B.T. Development, Characterization and the Application of Hybrid Materials in Coagulation/Flocculation of Wastewater: A Review. *Chem. Eng. J.* **2012**, *203*, 370–386. [CrossRef]
9. Copelli, S.; Raboni, M.; Urbini, G. Water pollution: Biological oxidation and natural control techniques. In *Reference Module in Chemistry, Molecular Sciences and Chemical Engineering*; Elsevier: Waltham, MA, USA, 2015; pp. 1–28. ISBN 978-0-12-409547-2.

10. Mohammadi, S.Z.; Safari, Z.; Madady, N. A Novel Co₃O₄@SiO₂ Magnetic Nanoparticle-Nylon 6 for High Efficient Elimination of Pb(II) Ions from Wastewater. *Appl. Surf. Sci.* **2020**, *514*, 145873. [[CrossRef](#)]
11. ISO/TR 18401:2017; Nanotechnologies—Plain Language Explanation of Selected Terms from the ISO/IEC 80004 Series 2017. ISO: Geneva, Switzerland, 2017.
12. Ma, M.; Hou, P.; Zhang, P.; Cao, J.; Liu, H.; Yue, H.; Tian, G.; Feng, S. Magnetic Fe₃O₄ Nanoparticles as Easily Separable Catalysts for Efficient Catalytic Transfer Hydrogenation of Biomass-Derived Furfural to Furfuryl Alcohol. *Appl. Catal. A Gen.* **2020**, *602*, 117709. [[CrossRef](#)]
13. Svoboda, J.; Fujita, T. Recent Developments in Magnetic Methods of Material Separation. *Miner. Eng.* **2003**, *16*, 785–792. [[CrossRef](#)]
14. Tang, S.C.N.; Lo, I.M.C. Magnetic Nanoparticles: Essential Factors for Sustainable Environmental Applications. *Water Res.* **2013**, *47*, 2613–2632. [[CrossRef](#)]
15. Wang, Q.; Guan, Y.; Ren, X.; Yang, M.; Liu, X. Application of Magnetic Extractant for the Removal of Hexavalent Chromium from Aqueous Solution in High Gradient Magnetic Separator. *Chem. Eng. J.* **2012**, *183*, 339–348. [[CrossRef](#)]
16. Torretta, V.; Urbini, G.; Raboni, M.; Copelli, S.; Viotti, P.; Luciano, A.; Mancini, G. Effect of Powdered Activated Carbon to Reduce Fouling in Membrane Bioreactors: A Sustainable Solution. Case Study. *Sustainability* **2013**, *5*, 1501–1509. [[CrossRef](#)]
17. Tuutijärvi, T.; Lu, J.; Sillanpää, M.; Chen, G. As(V) Adsorption on Maghemite Nanoparticles. *J. Hazard. Mater.* **2009**, *166*, 1415–1420. [[CrossRef](#)] [[PubMed](#)]
18. Raganati, F.; Alfe, M.; Gargiulo, V.; Chirone, R.; Ammendola, P. Kinetic Study and Breakthrough Analysis of the Hybrid Physical/Chemical CO₂ Adsorption/Desorption Behavior of a Magnetite-Based Sorbent. *Chem. Eng. J.* **2019**, *372*, 526–535. [[CrossRef](#)]
19. Wang, X.S.; Zhu, L.; Lu, H.J. Surface Chemical Properties and Adsorption of Cu (II) on Nanoscale Magnetite in Aqueous Solutions. *Desalination* **2011**, *276*, 154–160. [[CrossRef](#)]
20. Sobhanardakani, S.; Zandipak, R. Synthesis and Application of TiO₂/SiO₂/Fe₃O₄ Nanoparticles as Novel Adsorbent for Removal of Cd(II), Hg(II) and Ni(II) Ions from Water Samples. *Clean Technol. Environ. Policy* **2017**, *19*, 1913–1925. [[CrossRef](#)]
21. Hu, J.; Chen, G.; Lo, I.M.C. Removal and Recovery of Cr(VI) from Wastewater by Maghemite Nanoparticles. *Water Res.* **2005**, *39*, 4528–4536. [[CrossRef](#)]
22. Mahdavian, A.R.; Mirrahimi, M.A.-S. Efficient Separation of Heavy Metal Cations by Anchoring Polyacrylic Acid on Superparamagnetic Magnetite Nanoparticles through Surface Modification. *Chem. Eng. J.* **2010**, *159*, 264–271. [[CrossRef](#)]
23. Ozmen, M.; Can, K.; Arslan, G.; Tor, A.; Cengeloglu, Y.; Ersoz, M. Adsorption of Cu(II) from Aqueous Solution by Using Modified Fe₃O₄ Magnetic Nanoparticles. *Desalination* **2010**, *254*, 162–169. [[CrossRef](#)]
24. Hu, X.; Lei, H.; Zhang, X.; Zhang, Y. Strong Hydrophobic Interaction between Graphene Oxide and Supported Lipid Bilayers Revealed by AFM: Hydrophobic Interaction between GO and SLBS. *Microsc. Res. Tech.* **2016**, *79*, 721–726. [[CrossRef](#)]
25. Dreyer, D.R.; Park, S.; Bielawski, C.W.; Ruoff, R.S. The Chemistry of Graphene Oxide. *Chem. Soc. Rev.* **2010**, *39*, 228–240. [[CrossRef](#)]
26. Awad, A.M.; Jalab, R.; Benamor, A.; Nasser, M.S.; Ba-Abbad, M.M.; El-Naas, M.; Mohammad, A.W. Adsorption of Organic Pollutants by Nanomaterial-Based Adsorbents: An Overview. *J. Mol. Liq.* **2020**, *301*, 112335. [[CrossRef](#)]
27. Chen, D.; Feng, H.; Li, J. Graphene Oxide: Preparation, Functionalization, and Electrochemical Applications. *Chem. Rev.* **2012**, *112*, 6027–6053. [[CrossRef](#)]
28. Liu, X.; Ma, R.; Wang, X.; Ma, Y.; Yang, Y.; Zhuang, L.; Zhang, S.; Jehan, R.; Chen, J.; Wang, X. Graphene Oxide-Based Materials for Efficient Removal of Heavy Metal Ions from Aqueous Solution: A Review. *Environ. Pollut.* **2019**, *252*, 62–73. [[CrossRef](#)] [[PubMed](#)]
29. McCoy, T.M.; Brown, P.; Eastoe, J.; Tabor, R.F. Noncovalent Magnetic Control and Reversible Recovery of Graphene Oxide Using Iron Oxide and Magnetic Surfactants. *ACS Appl. Mater. Interfaces* **2015**, *7*, 2124–2133. [[CrossRef](#)] [[PubMed](#)]
30. Diagboya, P.N.; Olu-Owolabi, B.I.; Adebowale, K.O. Synthesis of Covalently Bonded Graphene Oxide–Iron Magnetic Nanoparticles and the Kinetics of Mercury Removal. *RSC Adv.* **2015**, *5*, 2536–2542. [[CrossRef](#)]
31. Cheng, Z.; Gao, Z.; Ma, W.; Sun, Q.; Wang, B.; Wang, X. Preparation of Magnetic Fe₃O₄ Particles Modified Sawdust as the Adsorbent to Remove Strontium Ions. *Chem. Eng. J.* **2012**, *209*, 451–457. [[CrossRef](#)]
32. Mahesh, N.; Balakumar, S.; Shyamalagowri, S.; Manjunathan, J.; Pavithra, M.K.S.; Babu, P.S.; Kamaraj, M.; Govarthanan, M. Carbon-Based Adsorbents as Proficient Tools for the Removal of Heavy Metals from Aqueous Solution: A State of Art-Review Emphasizing Recent Progress and Prospects. *Environ. Res.* **2022**, *213*, 113723. [[CrossRef](#)]
33. Barozzi, M.; Scotton, M.; Sieni, E.; Sgarbossa, P.; Sandon, A.; Copelli, S. Magnetically Separable Nanoparticles for Wastewater Treatment. *Chem. Eng. Trans.* **2021**, *86*, 1033–1038. [[CrossRef](#)]
34. Yaseen, D.A.; Scholz, M. Textile Dye Wastewater Characteristics and Constituents of Synthetic Effluents: A Critical Review. *Int. J. Environ. Sci. Technol.* **2019**, *16*, 1193–1226. [[CrossRef](#)]
35. Ghasemi, E.; Mirhabibi, A.; Edrissi, M. Synthesis and Rheological Properties of an Iron Oxide Ferrofluid. *J. Magn. Magn. Mater.* **2008**, *320*, 2635–2639. [[CrossRef](#)]
36. Pendolino, F.; Armata, N.; Masullo, T.; Cuttitta, A. Temperature Influence on the Synthesis of Pristine Graphene Oxide and Graphite Oxide. *Mater. Chem. Phys.* **2015**, *164*, 71–77. [[CrossRef](#)]
37. Liu, J.; Chen, Y.; Jiang, S.; Huang, J.; Lv, Y.; Liu, Y.; Liu, M. Rapid Removal of Cr(III) from High-Salinity Wastewater by Cellulose-g-Poly-(Acrylamide-Co-Sulfonic Acid) Polymeric Bio-Adsorbent. *Carbohydr. Polym.* **2021**, *270*, 118356. [[CrossRef](#)] [[PubMed](#)]

38. Azam, M.; Wabaidur, S.M.; Khan, M.R.; Al-Resayes, S.I.; Islam, M.S. Removal of Chromium(III) and Cadmium(II) Heavy Metal Ions from Aqueous Solutions Using Treated Date Seeds: An Eco-Friendly Method. *Molecules* **2021**, *26*, 3718. [[CrossRef](#)]
39. Kayalvizhi, K.; Alhaji, N.M.I.; Saravanakkumar, D.; Mohamed, S.B.; Kaviyarasu, K.; Ayeshamariam, A.; Al-Mohaimed, A.M.; AbdelGawwad, M.R.; Elshikh, M.S. Adsorption of Copper and Nickel by Using Sawdust Chitosan Nanocomposite Beads—A Kinetic and Thermodynamic Study. *Environ. Res.* **2022**, *203*, 111814. [[CrossRef](#)] [[PubMed](#)]
40. Foo, K.Y.; Hameed, B.H. Insights into the Modeling of Adsorption Isotherm Systems. *Chem. Eng. J.* **2010**, *156*, 2–10. [[CrossRef](#)]
41. Langmuir, I. The Constitution and Fundamental Properties of Solids and Liquids. Part I. Solids. *J. Am. Chem. Soc.* **1916**, *38*, 2221–2295. [[CrossRef](#)]
42. Sieni, E.; Di Barba, P.; Forzan, M. Migration NSGA: Method to Improve a Non-Elitist Searching of Pareto Front, with Application in Magnetics. *Inverse Probl. Sci. Eng.* **2016**, *24*, 543–566. [[CrossRef](#)]
43. Deb, K.; Pratap, A.; Agarwal, S.; Meyarivan, T. A Fast and Elitist Multiobjective Genetic Algorithm: NSGA-II. *IEEE Trans. Evol. Comput.* **2002**, *6*, 182–197. [[CrossRef](#)]